

Clinically feasible diffusion MRI in muscle: time dependence and initial findings in Duchenne Muscular Dystrophy

Amy R McDowell¹, Thorsten Feiweier², Francesco Muntoni^{3; 4}, Matt G Hall^{1,5}, Chris A Clark¹

Affiliations

¹Developmental Imaging and Biophysics, University College London, London, United Kingdom; ²Siemens Healthcare GmbH, Erlangen, Germany; ³UCL GOS Institute of Child Health, University College London, London, United Kingdom; ⁴NIHR Great Ormond Street Hospital Biomedical Research Centre, Great Ormond Street Institute of Child Health, University College London, & Great Ormond Street Hospital Trust, London, UK; ⁵National Physical Laboratory, London, United Kingdom

Address correspondence to:

*Dr Amy McDowell, Developmental Imaging and Biophysics, UCL GOS Institute of Child Health, 30 Guilford St, London, WC1N 1EH, UK
E mail: a.mcdowell@ucl.ac.uk; Tel 0207 905 2192; Orchid No. 0000-0002-4886-6191

Type of manuscript: Note

Word Count: 3102

Running Title: Time-dependant Diffusion MRI in Muscle

Acknowledgements

MGH and AM are part-supported by a grant from Great Ormond St Hospital's Biomedical Research Centre. AM is also supported by a grant from the National Physical Laboratory.

Disclosures

Thorsten Feiweier is an employee of Siemens Healthcare GmbH, owns stocks of Siemens (Healthineers) AG and holds patents filed by Siemens

Ethics

Ethical approval was granted for this study (12/LO/0442)

Authorship

All authors have made substantial contributions to 1) conception and design, or acquisition of data, or analysis and interpretation of data; 2) drafting the article or revising it critically for important intellectual content; and 3) final approval of the version to be published.

Abstract

Purpose

To characterise the diffusion time-dependence in muscle in healthy adult volunteers, boys with Duchenne's muscular dystrophy (DMD) and age-matched controls in a clinically feasible acquisition time for paediatric applications.

Methods

Diffusion data were acquired using a pulsed gradient stimulated echo diffusion preparation at five different diffusion times (70, 130, 190, 250, 330ms), at four different b-values (0, 200, 400, 600, and 800 s/mm²) and six directions (orthogonal x, y, and z and diagonal xy, xz, and yz) and processed to obtain standard diffusion indices (mean diffusivity (MD) and fractional anisotropy (FA)) at each diffusion time.

Results

Time dependant diffusion was seen in muscle in healthy adult volunteers, boys with DMD and age-matched controls. Boys with DMD showed reduced MD and increased FA values in comparison to age matched controls across a range of diffusion times. A diffusion time of $\Delta=190\text{ms}$ had the largest effect size.

Conclusions

These results could be used to optimise diffusion imaging in this disease further and imply that these diffusion indices may become an important biomarker in monitoring progression in DMD in the future.

Introduction

Duchenne muscular dystrophy (DMD) is a severe, progressive neuromuscular disorder for which multiple clinical trials are underway. In view of the variability of clinical course, fat-fraction and muscle T2-signal intensities have been proposed as non-invasive biomarkers for clinical trials and monitoring disease progression in DMD. These studies are encouraging and place muscle MRI at the centre of the efforts to develop novel, non-invasive biomarkers. Diffusion MRI is used extensively for applications in the brain but less commonly to investigate the microstructure of muscle. Diffusion MRI has the potential to provide a robust and sensitive biomarker for monitoring conditions such as muscular dystrophy¹⁻³ and other pathologies affecting muscle tissue by revealing changes in tissue microstructure.

Muscle fibres are much larger than brain white-matter axons and have a complex hierarchical internal structure⁴. They are comprised of myofibers which are 1 – 40 mm in length and 10 – 50 μm in width; these are packed with myofibrils which are in turn made up of myofilaments - chains of sarcomeres 2 μm in length, arranged end-to-end in bundles⁵. This is unlike axons which have mainly been modelled as empty cylinders⁶, assuming intra-axonal diffusion is unhindered along the axis of the cylinders, or only hindered perpendicular to the fibre axis by an external membrane^{7,8}.

Complex configurations or barriers to diffusion are known to form an environment in which diffusion may exhibit a time-dependence⁹. The presence of hierarchical structure in human muscle leads to a marked decrease in the observed diffusion coefficient with diffusion time in-vivo^{10,11}, which we have also recently demonstrated in murine muscle in-vivo¹². The diffusion time-dependence is sensitive to changes in the internal microstructure of muscle and therefore likely to be a good candidate as a probe of microstructural change due to the effects of pathology. Pathological changes may include: increase or decrease in number, size or permeability of the muscle fibres, inflammation and fibroadipose tissue infiltration. Sensitivity to several of these changes has been demonstrated previously after a 12-week exercise program in the human calf muscle¹³. An example clinical application would be an optimal diffusion time for the most sensitive measurement of the effects of pathology on the apparent diffusion coefficient.

Diffusion time sensitivity in muscle has been demonstrated by varying diffusion time with a constant b-value to make fibre diameter estimates in human calf muscle^{13,14}. Despite these observations, however, characterising the diffusion time-dependence in muscle requires a large number of acquisitions and can lead to clinically unacceptably long acquisition times. In this study, we describe an optimised diffusion acquisition protocol based on a vendor-provided prototype sequence implemented on a clinical 3T MRI system.

Experiments were conducted to examine the time-dependence of the diffusivity $D(t)$ at several b-values in the human calf muscle of healthy adult volunteers, boys with DMD and age-matched controls in a clinically feasible scan time considering the paediatric population. The age range of boys with DMD scanned was between 6 and 9 years as the protocol was designed to examine microstructural changes before substantial fat infiltration of muscle tissue is expected to occur.

In order to assess a wide range of diffusion times whilst minimising T2-decay, a Pulsed Gradient STimulated Echo (PGSTE) diffusion preparation was employed. This has the advantage of avoiding T2-relaxation effects during the mixing time as the magnetisation is stored in the longitudinal direction between the diffusion gradient pulses. This allows the acquisition of relatively long diffusion times without losing signal from T2-dephasing. For validation of the sequence, diffusion indices were measured in a water-only phantom, where mean diffusivity (MD) and fractional anisotropy (FA) were expected to remain constant with diffusion time. The use of the PGSTE preparation requires precise sequence design as unwanted diffusion-weighting from crusher and slice-select gradients may result without consideration; this is detailed in the methods section below.

Methods

PGSTE Preparation signal analysis

As the signal is lost more rapidly in muscle than brain due to shorter T2 values¹⁵⁻¹⁷ and higher diffusivity, it was important to utilise a TE under 100 ms and employ low b-values (below 1000 s/mm²) to ensure there was adequate signal in the images. The use of the PGSTE preparation in the diffusion sequence facilitates long diffusion times with short TE¹⁸. However, the PGSTE preparation may suffer unwanted diffusion-weighting from crusher and slice-select gradients which must be accounted for by careful sequence design and the use of a b-matrix corrected for 'cross terms' in the analysis of the images¹⁹; otherwise the signal may be biased at low b-values.

This study uses an optimised diffusion acquisition protocol based on a prototype sequence provided by the vendor, which combines a Pulsed Gradient STimulated Echo (PGSTE) diffusion preparation with an echoplanar imaging module (EPI). It has a similar spoiling scheme to Kleinnijenhuis et al.¹⁸ and was first utilised in Noehren et al.²⁰ It employs balanced slice-select gradients yielding a vanishing 0th moment during the mixing time, thus mitigating their impact on diffusion encoding. A pair of crusher gradients are applied if the implicit spoil moment of the diffusion-encoding gradients becomes insufficient to suppress signal contributions from undesired coherence pathways, as for example from the free induction decays generated by each of the applied RF pulses. Given the long duration between the two gradients, even small spoil moments will generate a non-negligible diffusion weighting, and all adverse contributions are considered when calculating the b-matrices used by the tensor estimations. These adverse contributions include all gradients of the diffusion-encoding module (diffusion gradients, crusher gradients (if any), slice-selection gradients) which affect the transversal magnetisation (this excludes any gradients applied between the centres of the store/restore RF-pulses). The b-matrices are calculated by the sequence and provided in the DICOM header for use by off-line processing programs.

PGSTE Preparation Validation – Water-only Phantom Measurements

Data were acquired on a clinical 3T scanner (MAGNETOM Prisma, Siemens Healthcare, Erlangen, Germany) using a 64-channel head coil. A PGSTE diffusion preparation in combination with an echoplanar imaging module was used. Scanning took place at room

temperature. This set of images was acquired to verify there was no intrinsic bias in the PGSTE preparation by measuring the MD and FA in a de-ionised water-filled falcon tube placed in a water bath at each diffusion time.

Diffusion data were acquired with a PGSTE preparation with pulse duration 10 ms and 7 diffusion times (Δ) of 52, 100, 150, 200, 250, 300 and 350 ms, each acquired at b-values of 0, 800, 1000, 1200, 1400, 1800 and 2000 s/mm². For the b=0 image, the actual b-value (obtained from the corrected b-matrix) varied from 10 s/mm² for Δ =52 ms, up to 90 s/mm² for Δ =350 ms due to contributions from the imaging gradients. Voxel size was 2x2 mm² with a slice thickness of 3 mm (matching the parameters used for in-vivo measurements as described below), and a TE and TR of 50 ms and 2500 ms, respectively. This acquisition set was repeated in the same session with 24 non-collinear directions and a 6-direction set from the in-vivo acquisition (see in-vivo measurements section).

In-vivo Measurements - Volunteers

Six healthy volunteers (4 females, 2 males; range 24-49 years old; average 35 years old) were imaged using a 15-channel knee coil. Volunteers were positioned with their right calf in the centre of the coil in the feet-first supine position. PGSTE diffusion data were acquired with pulse duration (δ) 10ms at 5 different diffusion times of 70, 130, 190, 250, 330 ms in each of 6 directions (orthogonal x, y, and z and diagonal xy, xz, and yz). B-values of 0, 200, 400, 600, and 800 s/mm² with 1, 4, 5, 6, 6 averages respectively were used. Voxel size was 2x2 mm² with a slice thickness of 3 mm, and a TE and TR of 50 ms and 2800 ms, respectively, with spectral attenuated inversion recovery fat suppression. For the b=0 image, the actual b-value (obtained from the corrected b-matrix) varied from 15 s/mm² for Δ =70 ms, up to 85 s/mm² for Δ =330 ms due to contributions from the imaging gradients. Acquisition time per diffusion time was 7:03 mins with a total time of 35:15 minutes. A water/fat separation sequence (T2-weighted fat-saturated turbo-spin-echo sequence, TE 73 ms, TR 3500 ms, pixel size 0.36x0.36 mm² with slice thickness of 3 mm) was also acquired to provide anatomical fat and water images.

In-vivo Measurements – Boys with DMD and Age-matched Controls

Five boys with DMD (range 6-9 years old; average 7.8 years old) and five age-matched male controls (range 6-10 years old; average 8.2 years old) were imaged with the same protocol as the volunteers described above. Ethical approval was granted for this study (12/LO/0442). The diagnosis of DMD was documented by genetic testing. The MR procedure was explained to the boys and they gave verbal consent, written consent was signed by a parent/legal guardian.

Acquisition time per diffusion time was again 7:03 mins with a total time of 35:15 minutes. Due to signal dropout caused by movement, one scan from a boy with DMD had to be excluded. Although the calf was held in place with padding, and the boys were verbally asked to keep as still as possible, the calf muscles can still be tensed during the acquisition, and this caused irreversible signal dropout in areas of the calf in this diffusion scan.

Phantom Data Processing

Data were pre-processed using Tractor (<http://www.tractor-mri.org.uk/>). The use of FSL topup and eddy correction was only possible using a 24-direction acquisition as these pre-processing steps require a minimum number of diffusion directions (details can be found in the FSL manual <https://fsl.fmrib.ox.ac.uk/fsl/fslwiki/eddy>). Six-direction data, matching the six directions used in the in-vivo work below, were extracted from the corrected 24-direction data to compare to the non-corrected six-direction data. Tensor fitting was performed at each diffusion time using FSL with a weighted least-squares fit. The acquisition sets were first processed with 24 directions, then 6 directions from the in-vivo acquisition, and finally 6 directions extracted from the 24 directions matching the 6 directions acquired in-vivo.

Volumes of interest (VOIs) were placed in the water phantom on the MD images reconstructed at the shortest diffusion time and then copied on to the rest of the maps using MIPAV (<https://mipav.cit.nih.gov/>). Signal-to-noise ratios (SNR) were also calculated on the raw data with a larger VOI in the water bath surrounding the falcon tube using two repeated diffusion images in the same gradient direction. SNR was calculated at two b-values (800 and 2000 s/mm²) using either the 24-direction set or the in-vivo 6-direction set at each diffusion time to assess the changes in signal as diffusion time is increased. This followed the methods for a repeated-image SNR measurement in the presence of multi-channel coils and parallel-imaging as detailed in Dietrich et al²¹.

In-vivo Data Processing

As with the phantom acquisitions, data were processed using Tractor, and tensor fitting was performed at each diffusion time using FSL using a weighted least-squares fit. VOIs were drawn using MIPAV in the tibialis anterior (TA) muscle on the B0 images at the shortest diffusion time with reference to the fat and water anatomical images.

As the main purpose of this pilot study was to study the microstructure and diffusion indices before fat infiltration when the muscle function may still be recoverable, the TA muscle was chosen for analysis due to its parallel and linear orientation to B0, and non-visible fat infiltration. Successful fat suppression nulls the fat signal across the field-of-view, mitigating the chemical shift artifact, but leads to muscles with greater fat infiltration typically exhibiting reduced signal and poorer SNR as just the contribution from water remains. Moreover, each of the four boys with DMD has different levels of fat infiltration in other muscles which would add another variable into this pilot group. An examination of these effects in the lateral gastrocnemius muscle is included in the Supporting Information and shown in Supporting Information Figure S4.

All images at all b-values were included to use all available data in the calculation as our experiment was not designed to provide the redundancy of data required to optimise for b-value, only to assess the effect of diffusion time. MD, FA and principal eigenvectors were analysed in each voxel of interest. Angular dispersion of eigenvectors was calculated relative to the spherical mean of all directions in the ROI using the dot product.

Results

PGSTE preparation Validation - Phantom Measurements

An analysis of any bias in the signal value due to unsuitable gradient application using the PGSTE preparation is given in the Supporting information. No unexpected signal changes were seen (Supporting Information Figure S1). Graphs of MD and FA calculated in the microstructure phantom and in free water for the 24-direction set, 6 directions extracted from the 24 directions matching the in-vivo 6-direction set, and the in-vivo 6-direction set is shown in Supporting Information Figure S2. The data using 24 directions shows less variation across the diffusion times in free water, but higher SNR and lower variance would be expected with extra data points. No significant time-dependence is observed for MD values in free water, but a small bias is observed – a difference of 0.03×10^{-3} in the means at $\Delta=52$ ms and 350 ms of the 24-direction set. It is likely that this is due to Rician bias (or alternatively a positive noise floor from a non-central Chi distribution of noise) from the increasing noise in the images with increasing diffusion time. Estimation and removal of noise in DWI images is non-trivial and imperfect, and as the error in tensor calculation with the 6-direction set used in-vivo is greater due to fewer data points, it was not performed. This bias is also observed for FA – a difference of 0.0037 in the means at $\Delta=52$ ms and 350ms of the 24-direction set. Signal-to-noise ratios calculated for one gradient direction at $b = 800$ and $b = 2000$ using either the 24-direction set or the 6-direction set are shown in Supporting Information Figure S3. We observed no apparent difference in SNR with diffusion time.

In-vivo measurements - Volunteers

Example fat, water, B0, MD and FA images from one male 39-year-old healthy volunteer are shown in Figure 1. The B0 image shows visible delineation of the muscle groups with acceptable distortion, though incomplete fat-suppression. Quantitative results are shown in Figure 2. The mean MD decreases from 1.31×10^{-3} mm²/s at $\Delta=70$ ms to 1.08×10^{-3} mm²/s at $\Delta=330$ ms. Mean FA increases from 0.31 at $\Delta=70$ ms to 0.40 at $\Delta=330$ ms. Significance between the minimum and maximum diffusion times was $P < 0.0001$ for MD and < 0.0001 for FA. Box plots for all diffusion parameters in healthy volunteers (MD, FA, λ_1 , λ_2 and λ_3) are shown in Supporting Information Figure S5.

Angular dispersion of eigenvectors was calculated relative to the spherical mean direction in the ROI using the dot product and is shown in Supporting Information Figure S6. We observed a mean angular deviation of 13.3 degrees (standard deviation (SD) 6.3 degrees) at $\Delta=70$ ms and of 12.3 degrees (SD 5.3 degrees) at 330 ms. There was no significant difference in angular dispersion between these two diffusion times ($P=0.63$).

In-vivo measurements – Controls and Boys with DMD

Example fat, water, B0, MD and FA images from a representative boy with DMD and representative age-matched control are shown in Figure 3. Fat infiltration is seen in the DMD images. Images of all participants at diffusion time 70 ms are shown in Supporting Information Figure S7. MD and FA images at all diffusion times from the boy with DMD and age-matched control in Figure 3 are shown in Supporting Information Figure S8.

Quantitative results for MD and FA are shown in Table 1 and graphically in Figure 4. Box plots for diffusion parameters in controls and boys with DMD (MD, FA, λ_1 , λ_2 and λ_3) are shown separately in Supporting Information Figures S9 and S10, respectively. In Table 1, we have calculated Cohen's-d effect size for MD and FA at each diffusion time. This provides a robust quantification of the observed differences in the data acquired; these are given as a guide for choice of diffusion parameters and power calculations for future studies.

Discussion

A time-dependent diffusion imaging protocol has been acquired in muscle in a clinically feasible scan time of 7 minutes per diffusion time for healthy adult volunteers, boys with DMD and in age-matched controls. Images are of good quality with acceptable fat suppression. MD showed a strong time-dependence in healthy muscle, decreasing with diffusion time, as expected. This is in agreement with the results found by Porcari et al in mice¹² and human measurements¹³. Fractional anisotropy also showed a distinct increase with diffusion time.

In this exploratory study, boys with DMD showed increased MD and decreased FA values in comparison to age-matched controls across a range of diffusion times in the TA muscle. This agrees with results by Hoojijmans et al.³. This implies a change in the microstructure, such as a possible increase in permeability of the injured muscle fibres with the corresponding decrease in directionality or FA as water passes more quickly between the microstructural compartments. The TA muscle was chosen for analysis as it has the most normal macroscopic appearance on the fat/water images in this set of early stage, still ambulatory boys with DMD. However, differences between normal and pathological muscle tissue diffusion indices are still seen at all diffusion times. Diffusion MRI is able to provide quantitative measures of alteration in microstructure before qualitative changes in appearance on anatomical images. A diffusion time of 190 ms had the largest effect size in separating control and disease states and is a basis for the optimisation of diffusion time for this patient group. Specifically, these results indicate that longer diffusion times than those routinely used in diffusion imaging (typically <100 ms) may maximise the sensitivity of conventional DTI metrics such as MD and FA for application as a biomarker in DMD. For example, the work by Porcari et al. found that the strongest differences in diffusion indices between a pathological mouse model of DMD and controls was at long diffusion times (>250 ms).

Further work to optimise the choice of b-values and the selection of a single diffusion time for specific study protocols will be useful - dependant on an individual centre's scanner capability and time available for scanning. A single b-value with a high number of directions (12 or more) may be found to provide sufficient information in a single acquisition. The lower b-values (200s/mm², 400s/mm²) require less averages to boost the reduced signal in the PGSTE sequence minimising acquisition time further.

This finding underlines the potential for diffusion MRI to become established in the future as an important biomarker in DMD and other similar neuromuscular pathologies. Further work with a larger number of patients is now required to confirm and extend these results. Such studies should carefully compare existing MRI biomarkers in DMD such as Dixon fat/water content and T2-measurements in comparison to long diffusion time MRI as described here.

Conclusion

We have demonstrated that time-dependent diffusion in muscle can be imaged in a clinically feasible scan time using modern clinical MRI equipment, and further that distinct differences are observed in diffusion metrics between boys with DMD and healthy controls. Further studies are now warranted in larger cohorts including comparison with existing MRI biomarkers such as T2-mapping and Dixon fat/water imaging.

References

1. Ponrartana S, Ramos-Platt L, Wren TA, et al. Effectiveness of diffusion tensor imaging in assessing disease severity in Duchenne muscular dystrophy: preliminary study. *Pediatric radiology*. 2015;45(4):582-589.
2. Li GD, Liang YY, Xu P, Ling J, Chen YM. Diffusion-Tensor Imaging of Thigh Muscles in Duchenne Muscular Dystrophy: Correlation of Apparent Diffusion Coefficient and Fractional Anisotropy Values With Fatty Infiltration. *AJR American journal of roentgenology*. 2016;206(4):867-870.
3. Hooijmans MT, Damon BM, Froeling M, et al. Evaluation of skeletal muscle DTI in patients with duchenne muscular dystrophy. *NMR in biomedicine*. 2015;28(11):1589-1597.
4. Feher J. 3.5 - Contractile Mechanisms in Skeletal Muscle. In: Feher J, ed. *Quantitative Human Physiology (Second Edition)*. Boston: Academic Press; 2017:305-317.
5. Lodish HB, A.; Kaiser, C.A.; Krieger, M.; Bretscher, A.; Ploegh, H.; Amon,A.; Martin, K.C. *Molecular Cell Biology*. 4th ed: W. H. Freeman; 2000.
6. Assaf Y, Blumenfeld-Katzir T, Yovel Y, Basser PJ. AxCaliber: a method for measuring axon diameter distribution from diffusion MRI. *Magnetic resonance in medicine*. 2008;59(6):1347-1354.
7. Alexander DC, Hubbard PL, Hall MG, et al. Orientationally invariant indices of axon diameter and density from diffusion MRI. *NeuroImage*. 2010;52(4):1374-1389.
8. Zhang H, Schneider T, Wheeler-Kingshott CA, Alexander DC. NODDI: practical in vivo neurite orientation dispersion and density imaging of the human brain. *NeuroImage*. 2012;61(4):1000-1016.
9. Novikov DS, Fieremans E, Jensen JH, Helpert JA. Random walk with barriers. *Nat Phys*. 2011;7(6):508-514.
10. Marschar AM, Kuder TA, Stieltjes B, Nagel AM, Bachert P, Laun FB. In vivo imaging of the time-dependent apparent diffusional kurtosis in the human calf muscle. *Journal of magnetic resonance imaging : JMRI*. 2015;41(6):1581-1590.
11. McDowell AR, Hall MG, Feiweier T, Clark CA. Time-dependent diffusion in healthy human calf muscle in a clinically feasible acquisition time. Paper presented at: 20th Annual meeting of ISMRM2020; Online.
12. Porcari P, Hall MG, Clark CA, Grealley E, Straub V, Blamire AM. Time-dependent diffusion MRI as a probe of microstructural changes in a mouse model of Duchenne muscular dystrophy. *NMR in biomedicine*. 2020:e4276.
13. Fieremans E, Lemberskiy G, Veraart J, Sigmund EE, Gyftopoulos S, Novikov DS. In vivo measurement of membrane permeability and myofiber size in human muscle using time-dependent diffusion tensor imaging and the random permeable barrier model. *NMR in biomedicine*. 2017;30(3).
14. Sigmund EE, Novikov DS, Sui D, et al. Time-dependent diffusion in skeletal muscle with the random permeable barrier model (RPBM): application to normal controls and chronic exertional compartment syndrome patients. *NMR in biomedicine*. 2014;27(5):519-528.
15. Saupe N, White LM, Stainsby J, Tomlinson G, Sussman MS. Diffusion Tensor Imaging and Fiber Tractography of Skeletal Muscle: Optimization of b Value for Imaging at 1.5 T. *American Journal of Roentgenology*. 2009;192(6):W282-W290.

16. Casey S. "T2 Washout": An Explanation for Normal Diffusion-Weighted Images Despite Abnormal Apparent Diffusion Coefficient Maps. *American Journal of Neuroradiology*. 2001;22(8):1450.
17. Jordan CD, Saranathan M, Bangerter NK, Hargreaves BA, Gold GE. Musculoskeletal MRI at 3.0 T and 7.0 T: a comparison of relaxation times and image contrast. *European journal of radiology*. 2013;82(5):734-739.
18. Kleinnijenhuis M, Mollink J, Lam WW, et al. Choice of reference measurements affects quantification of long diffusion time behaviour using stimulated echoes. *Magnetic resonance in medicine*. 2018;79(2):952-959.
19. Lundell H, Alexander DC, Dyrby TB. High angular resolution diffusion imaging with stimulated echoes: compensation and correction in experiment design and analysis. *NMR in biomedicine*. 2014;27(8):918-925.
20. Noehren B, Andersen A, Feiweier T, Damon B, Hardy P. Comparison of twice refocused spin echo versus stimulated echo diffusion tensor imaging for tracking muscle fibers. *Journal of magnetic resonance imaging : JMRI*. 2015;41(3):624-632.
21. Dietrich O, Raya JG, Reeder SB, Reiser MF, Schoenberg SO. Measurement of signal-to-noise ratios in MR images: influence of multichannel coils, parallel imaging, and reconstruction filters. *Journal of magnetic resonance imaging : JMRI*. 2007;26(2):375-385.

Table and Figures

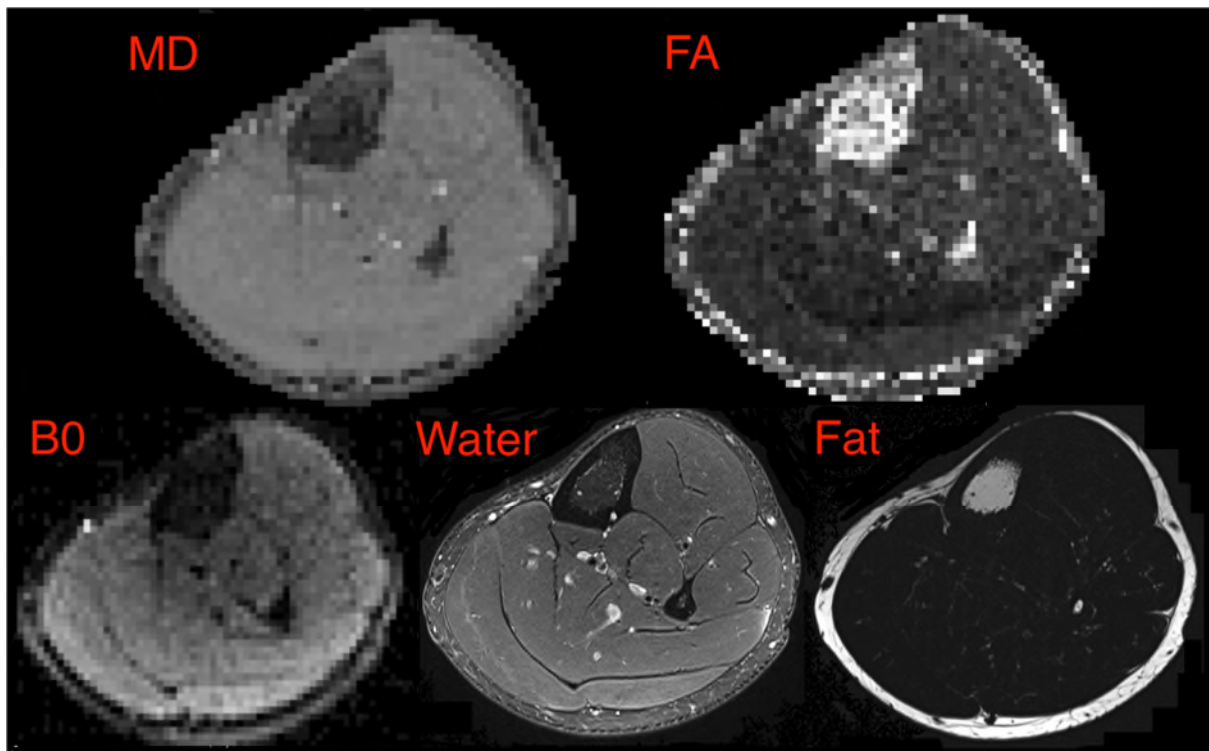


Figure 1: Example fat, water, B0, MD and FA images at diffusion time 70ms from one male 39-year-old healthy volunteer

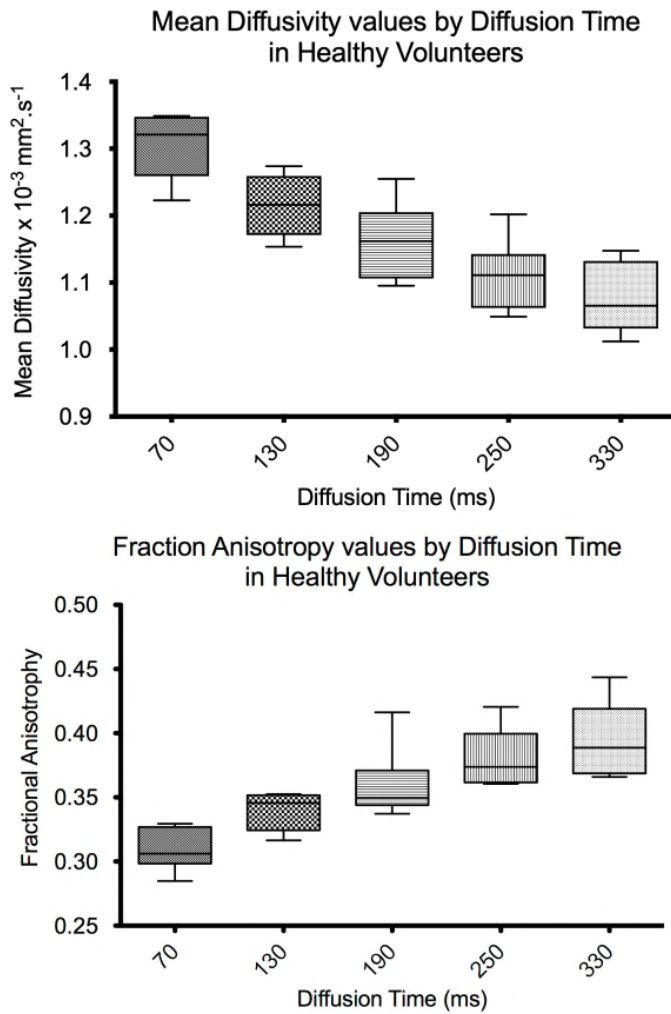


Figure 2: Box-and-whisker plots of MD and FA in healthy volunteers plotted by diffusion time. Whiskers are 5% to 95% percentile.

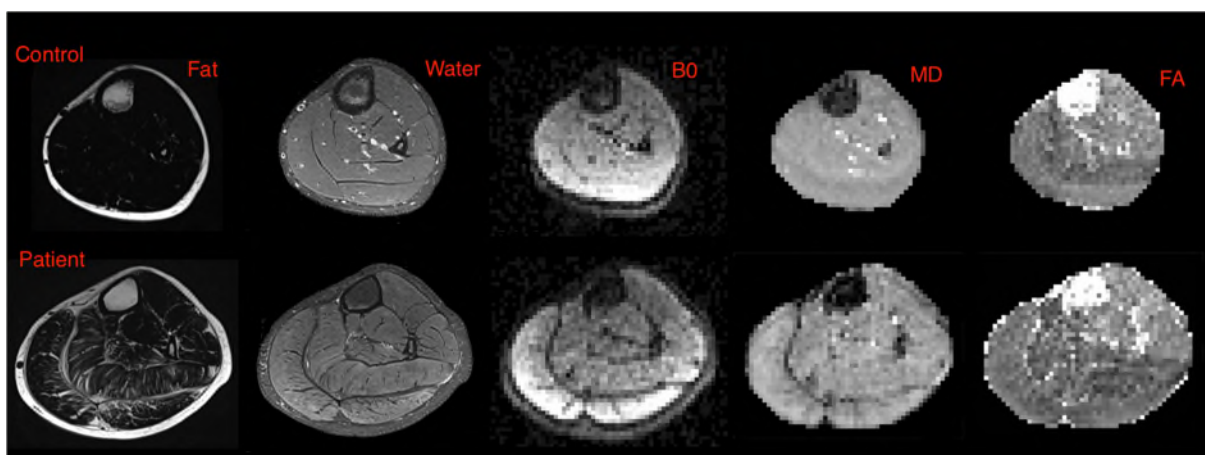


Figure 3: Example fat, water, B0, MD and FA images at diffusion time 70ms from a control participant (top row, age 8 years) and a boy with DMD (bottom row, age 8 years)

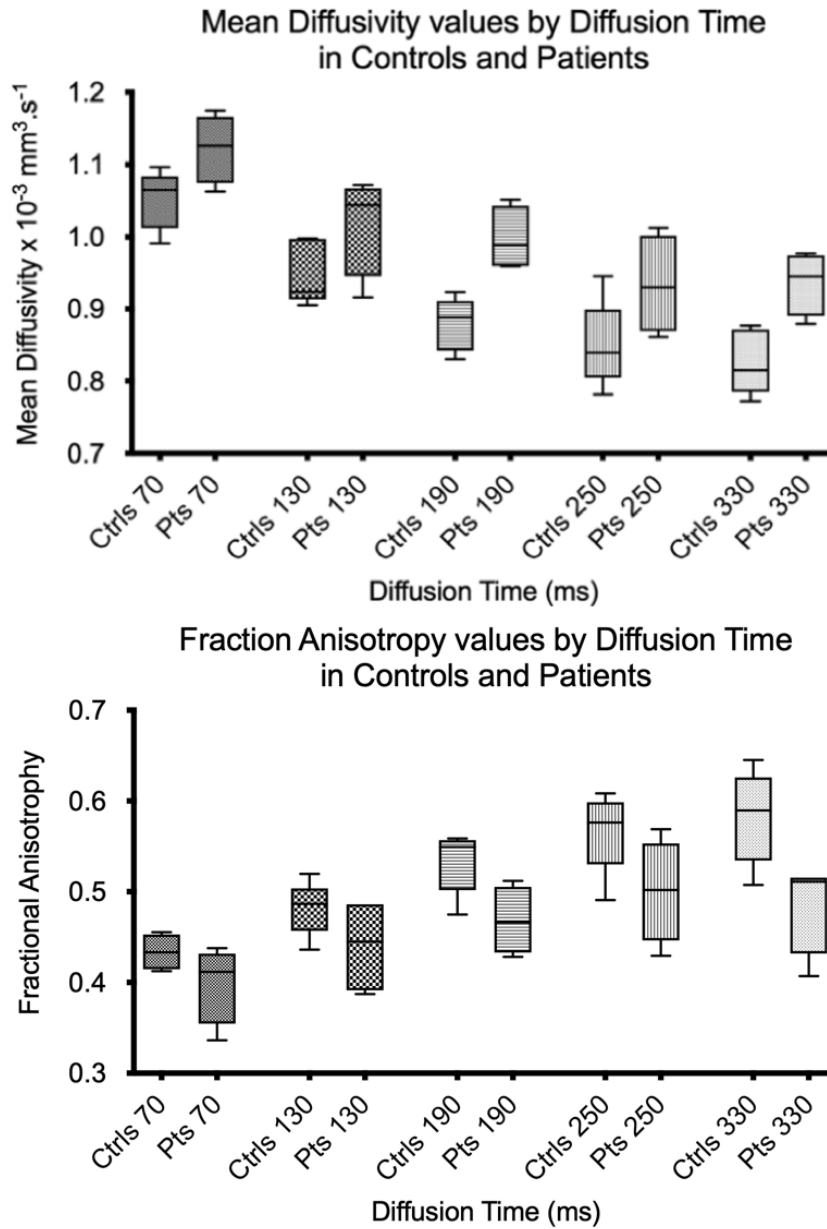


Figure 4: Box-and-whisker plots of MD and FA in controls and patients plotted by diffusion time. Whiskers are 5% to 95% percentile.

MD x 10⁻³ mm².s⁻¹	Δ=70ms	Δ=130ms	Δ=190ms	Δ=250ms	Δ=330ms
Controls	1.05±0.27	0.95±0.25	0.88±0.24	0.85±0.25	0.83±0.25
DMD	1.12±0.27	1.02±0.23	1.00±0.25	0.93±0.25	0.94±0.24
FA	Δ=70ms	Δ=130ms	Δ=190ms	Δ=250ms	Δ=330ms
Controls	0.43±0.16	0.48±0.18	0.53±0.18	0.57±0.18	0.58±0.19
DMD	0.40±0.13	0.44±0.14	0.47±0.14	0.50±0.18	0.49±0.17
Effect size	Δ=70ms	Δ=130ms	Δ=190ms	Δ=250ms	Δ=330ms
MD	0.88	1.08	3.96	0.69	1.60
FA	-0.57	-1.05	-1.89	-0.75	-1.26

Table 1 Average MD and FA values (± SD) in controls and boys with DMD for each diffusion time. Cohen's d effect sizes were calculated for controls and boys with DMD at each diffusion time to act as a guide to optimal diffusion time selection

Supporting Information Figure Captions

Supporting Information Figure S1: Signal values in a simple free-water phantom acquired using the PGSTE sequence over a range of b-values and diffusion times. Signal value data points are connected with a simple line rather than an exponential fit to demonstrate any step changes in signal more easily. Each data point is the average of 12 measurements, standard deviation values were between 1.1 and 7.9 with an average of 3.9 and therefore the error bars are not discernible on the graph.

Supporting Information Figure S2: Graphs of Mean Diffusivity values and Fractional Anisotropy in free water. Dataset for the 24-direction set is shown in blue, for 6-direction set in green, and the matched 6-direction set extracted from the 24-direction set in red. Error bars are one standard deviation

Supporting Information Figure S3: Signal-to-noise ratios for one gradient direction calculated at two b-values 800 and 2000 s/mm² for the 24-direction set and the in-vivo 6-direction set at each diffusion time

Supporting Information Figure S4: Box-and-whisker plots of MD and FA in controls and patients plotted by diffusion time in the lateral gastrocnemius muscle. Whiskers are 5% to 95% percentile.

Supporting Information Figure S5: Box-and-whisker plots of MD, FA and eigenvalues in healthy adult volunteers plotted by diffusion time in Tibialis Anterior muscle. Whiskers are 5% to 95% percentile.

Supporting Information Figure S6: Box-and-whisker plots of the distribution of angular deviation of the principal eigenvector from the spherical mean direction in degrees in healthy volunteers. Whiskers are 5% to 95% percentile.

Supporting Information Figure S7: Fat (F), water (W), B0, Mean Diffusivity (MD) and Fractional Anisotropy (FA) images at diffusion time 70ms of all age-matched controls (C) and Boys with Duchenne's (P). Regions of interest are shown on the B0 images.

Supporting Information Figure S8: Example control and patient images for all diffusion times in one control and one boy with DMD (as Figure 3 in main paper). Diffusion times were 70, 130, 190, 250 and 330ms. MD and FA images are scaled identically for all diffusion times (MD $0.0-0.2 \times 10^{-3} \text{ mm}^2 \text{ s}^{-1}$, FA 0.0-0.7)

Supporting Information Figure S9: Box-and-whisker plots of MD, FA and eigenvalues in healthy controls plotted by diffusion time in Tibialis Anterior muscle. Whiskers are 5% to 95% percentile

Supporting Information Figure S10: Box-and-whisker plots of MD, FA and eigenvalues in boys with DMD plotted by diffusion time in Tibialis Anterior muscle. Whiskers are 5% to 95% percentile

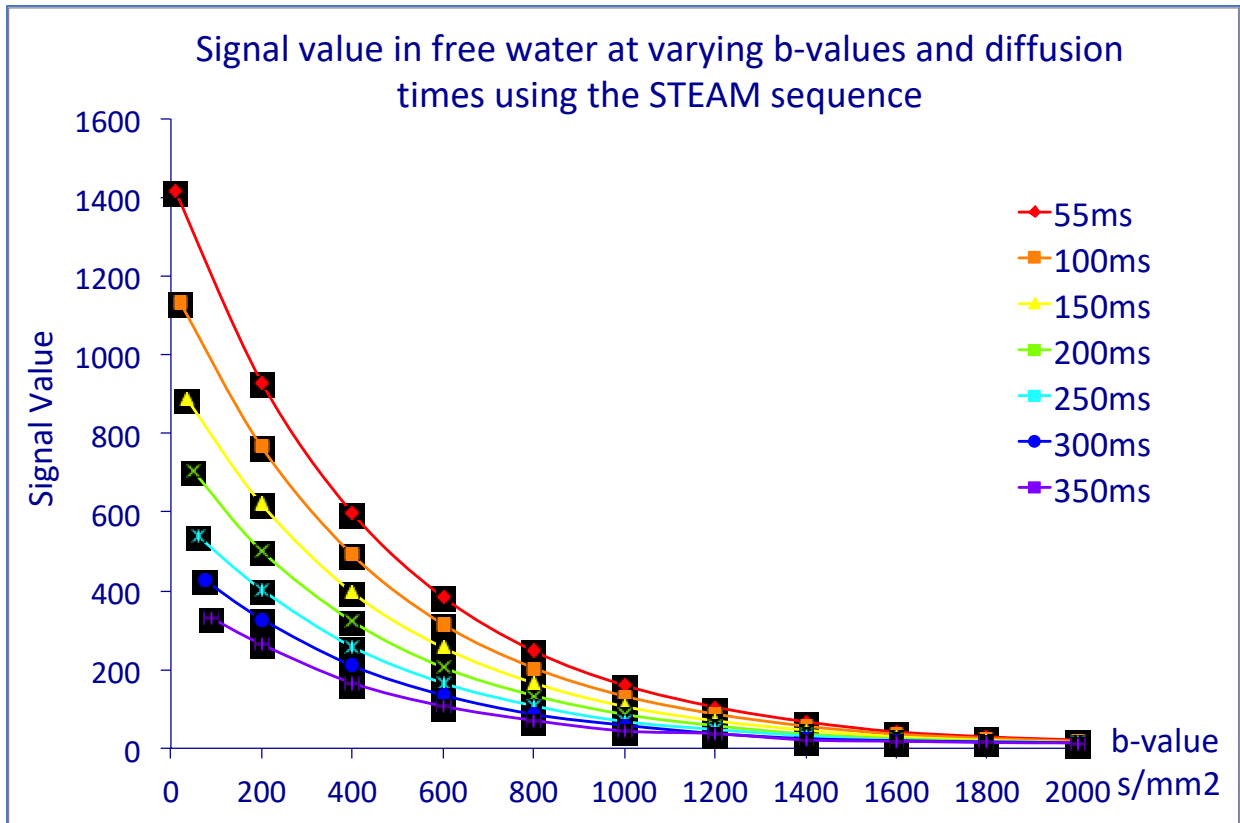
Supporting Information

PGSTE sequence signal analysis

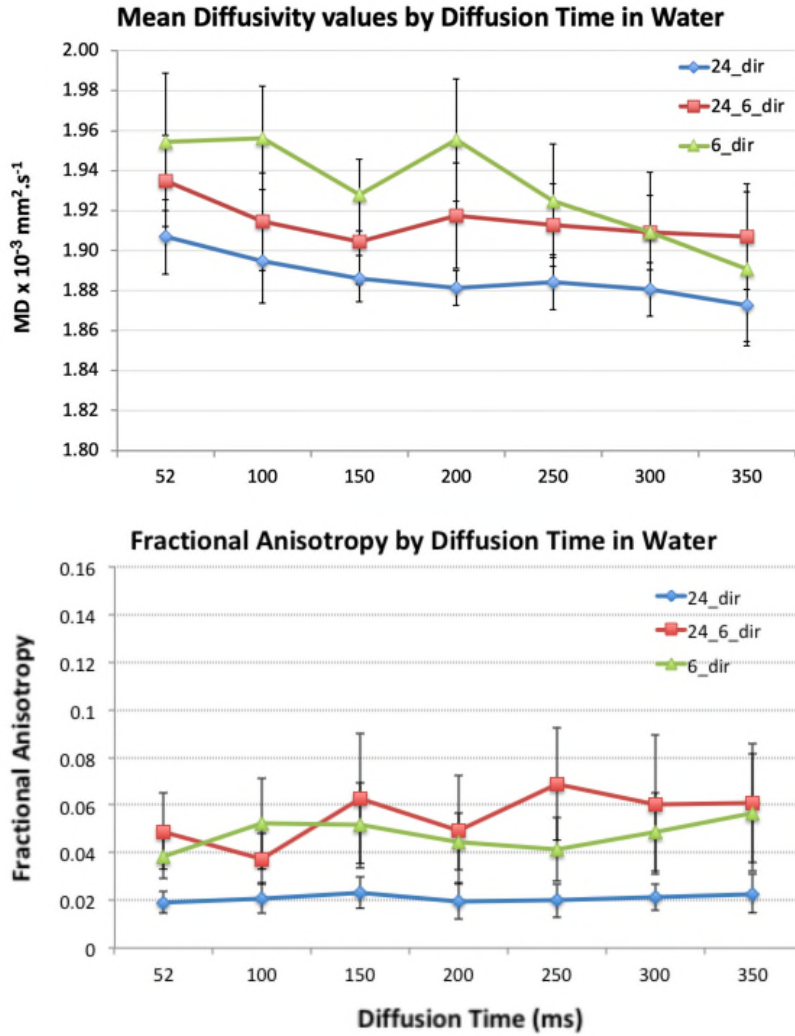
We expected that a switching of spoiler gradients (see methods section “PGSTE preparation signal analysis” in the main paper) between b-values would manifest as a step change in signal, and therefore an analysis of the acquired signal was undertaken (see methods section for details of management of the gradients in the PGSTE preparation). Data were acquired on a 3T MAGNETOM Prisma with a maximum gradient strength of 80 mT/m (Siemens Healthcare, Erlangen, Germany) using a 64-channel head coil in a simple free-water phantom consisting of a sample tube doped with gadolinium (0.2%). An IR-TSE T1 map was first acquired of the phantom (TR 12000ms; TE 13ms, and IR values of 400, 600, 1000, 1500 and 2000 ms) and the T1 calculated. This was found to be an average of 1405ms. The PGSTE sequence was applied over the range of expected b-values (0, 200, 400, 600, 800, 1000, 1200, 1400, 1600, 1800 and 2000s/mm²) and diffusion times (55, 100, 150, 200, 250, 300, 350 ms). Signal curves are plotted from a VOI placed over the signal tube for each diffusion time.

Results

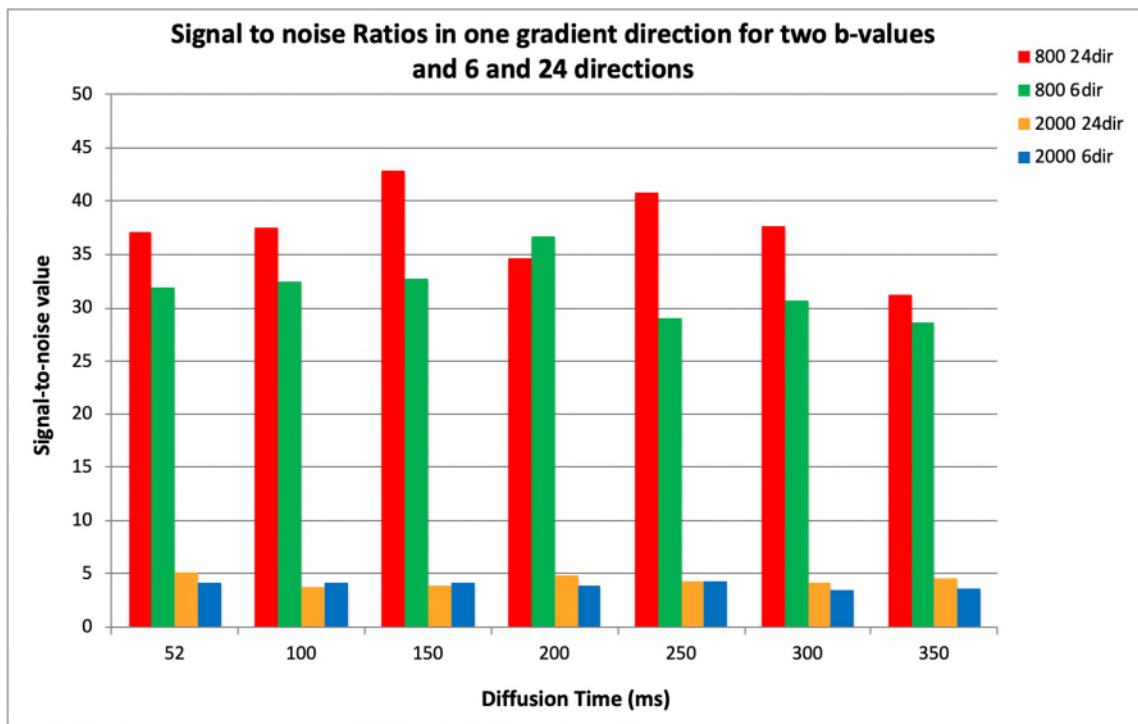
There were no unexpected signal changes in the diffusion signal value acquired using the free-water phantom (Supporting Information Figure S1). The curves are smooth with no unexpected step changes where the signal had been affected by a miscalculation of gradient application.



Supporting Information Figure S1: Signal values in a simple free-water phantom acquired using the PGSTE sequence over a range of b-values and diffusion times. Signal value data points are connected with a simple line rather than an exponential fit to demonstrate any step changes in signal more easily. Each data point is the average of 12 measurements, standard deviation values were between 1.1 and 7.9 with an average of 3.9 and are therefore the error bars are not discernible on the graph.



Supporting Information Figure S2: Graphs of Mean Diffusivity values and Fractional Anisotropy in free water. Dataset for the 24-direction set is shown in blue, for 6-direction set in green, and the matched 6-direction set extracted from the 24-direction set in red. Error bars are one standard deviation



Supporting Information Figure S3: Signal-to-noise ratios for one gradient direction calculated at two b-values 800 and 2000 s/mm² for the 24-direction set and the in-vivo 6-direction set at each diffusion time

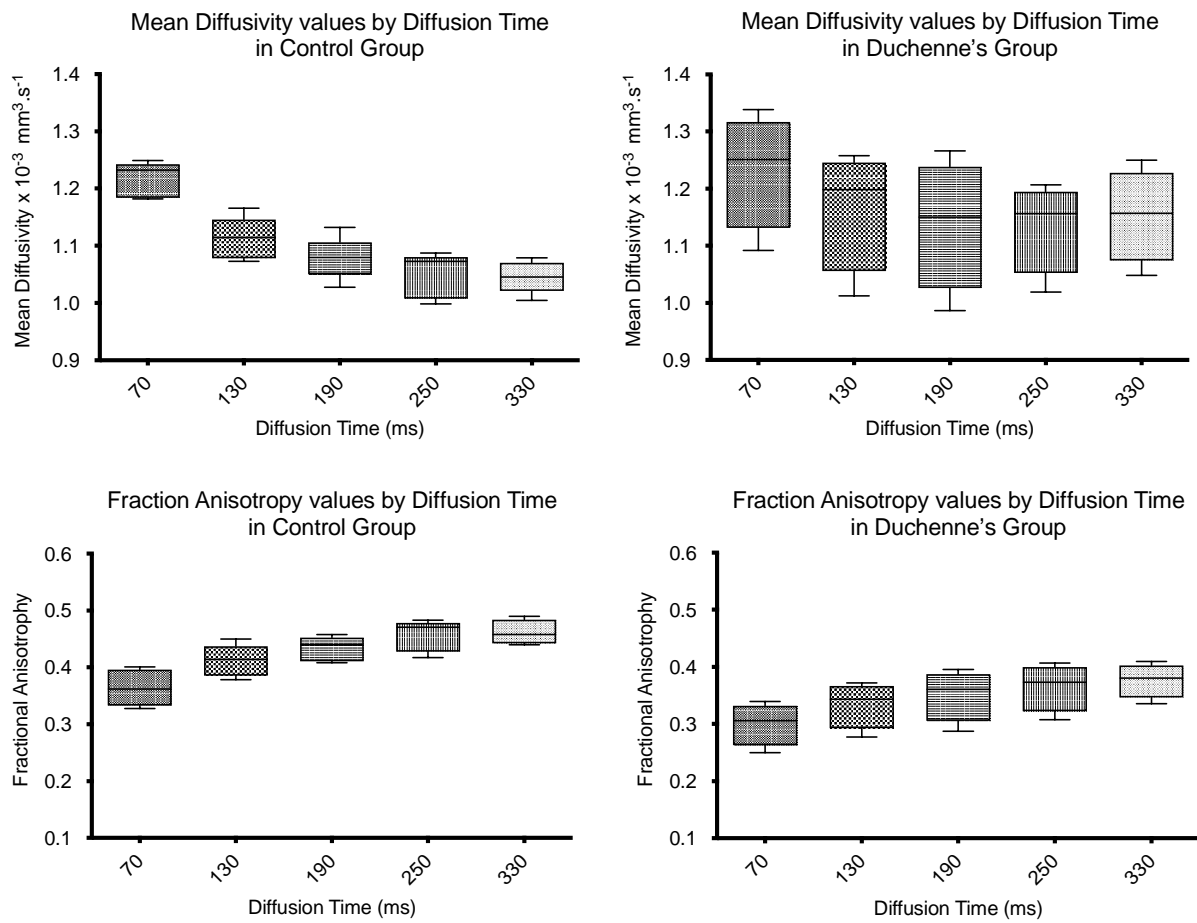
Choice of Region of Interest in Analysis for this paper

There are several reasons for choosing a macroscopically non-fat infiltrated muscle for analysis. Firstly, each of the four patients has different levels of fat infiltration in other muscles, introducing another variable into a small group. Secondly, muscle with greater fat infiltration typically exhibits reduced water diffusion signal resulting in reduced SNR. Shown below are the results for a ROI in the lateral gastrocnemius muscle. This muscle has varying levels of fat infiltration in each of the four patients, affecting the analysis.

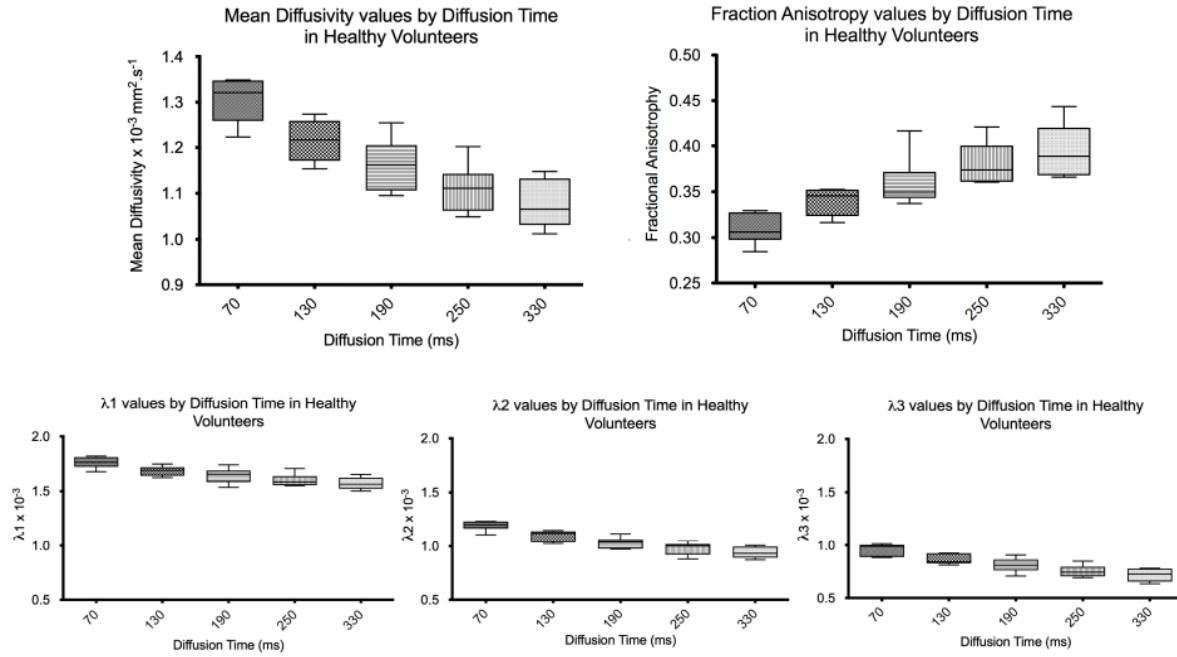
As can be seen in Supporting Information Figure S4 below, the control MD and FA indices are similar to TA muscle results, but the MD results exhibit larger variation. They are confounded by variation in fat infiltration, lack of signal, or a combination of both.

Interestingly, the FA results show less sensitivity, but as FA is lower in the patients it may not be as sensitive a measure overall. As the main purpose of this pilot study was to study the microstructure and diffusion indices before fat infiltration, when the muscle function may still be recoverable, we have concentrated on the TA muscle.

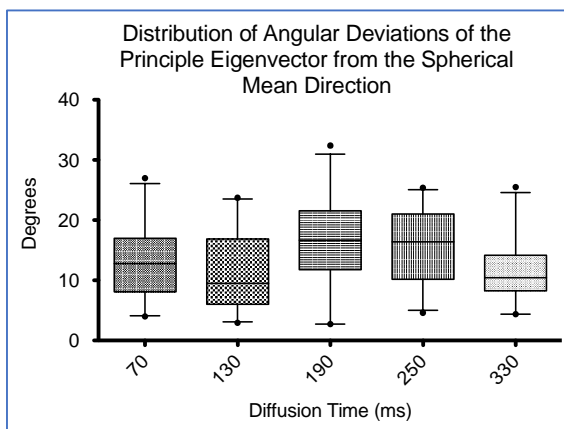
For further work, it is possible that in a larger group that fat infiltration could be assessed by a standard chemical shift method, the patients stratified into groups e.g., 0-10%, 10-20% etc. and the diffusion indices may be of interest. SNR would still be low, so perhaps using an optimised single b-value at an optimised diffusion time could boost the signal by adding more averages, but this is outside the scope of this project.



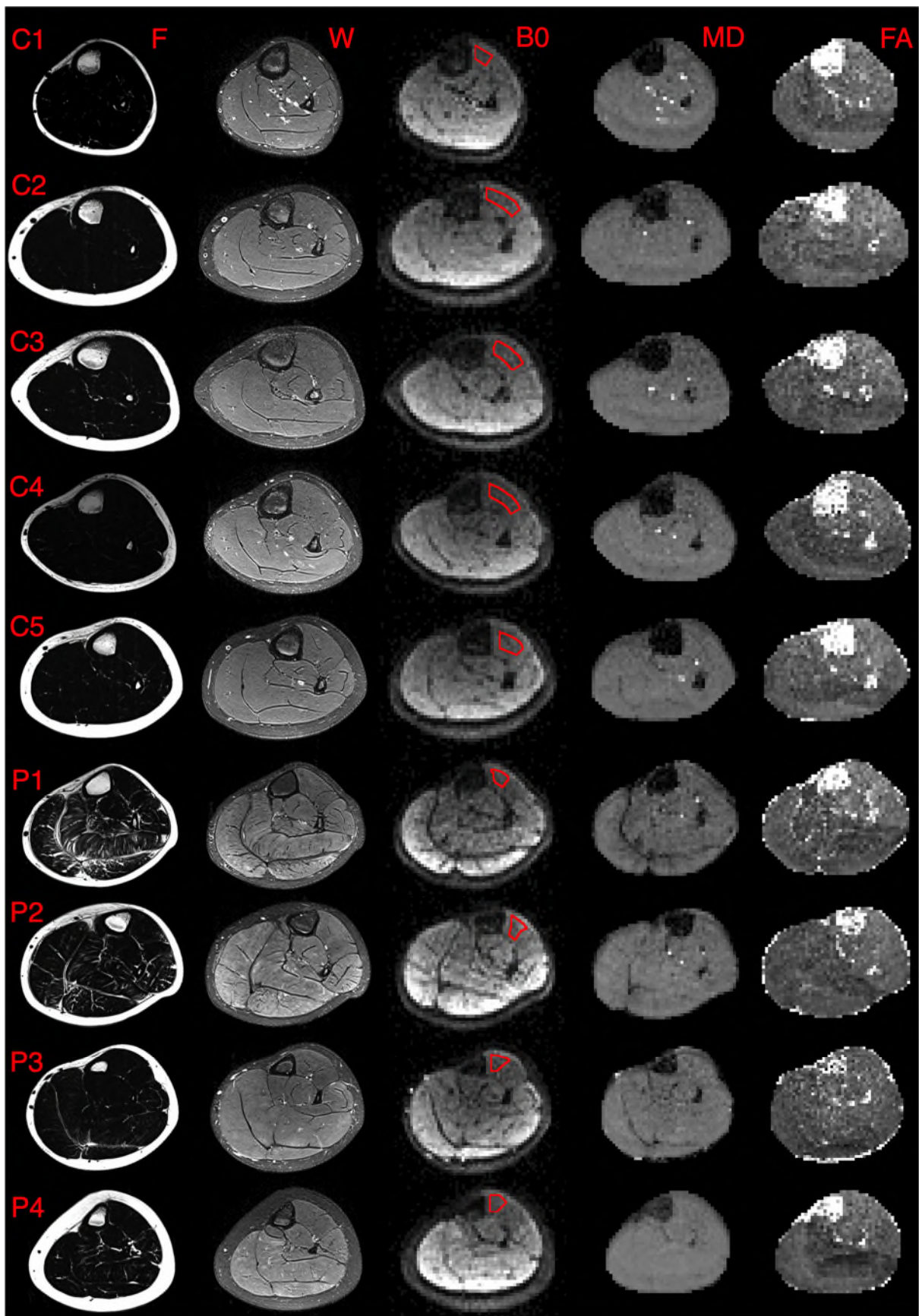
Supporting Information Figure S4: Box-and-whisker plots of MD and FA in controls and patients plotted by diffusion time in the lateral gastrocnemius muscle. Whiskers are 5% to 95% percentile.



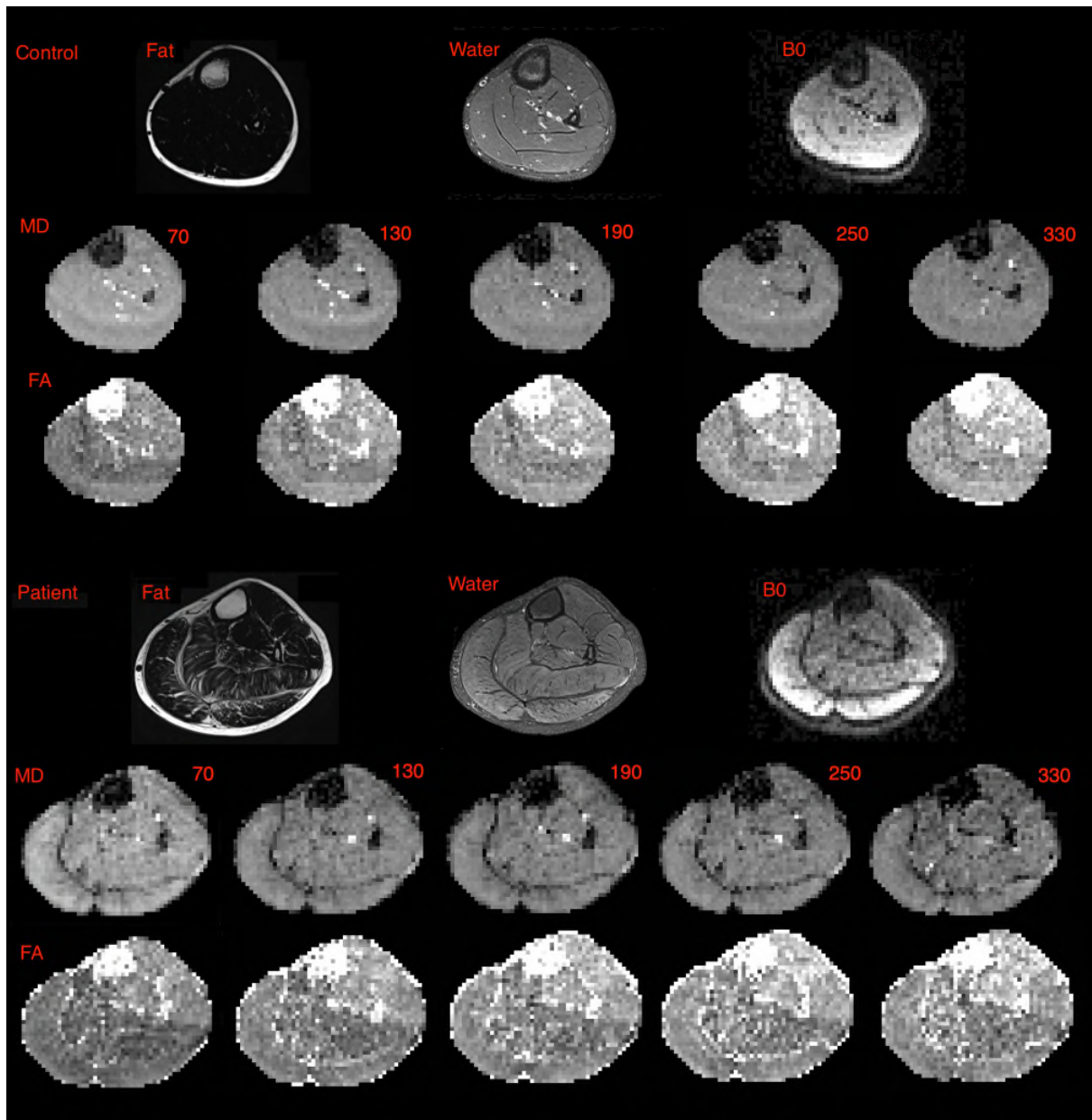
Supporting Information Figure S5: Box-and-whisker plots of MD, FA and eigenvalues in healthy adult volunteers plotted by diffusion time in Tibialis Anterior muscle. Whiskers are 5% to 95% percentile.



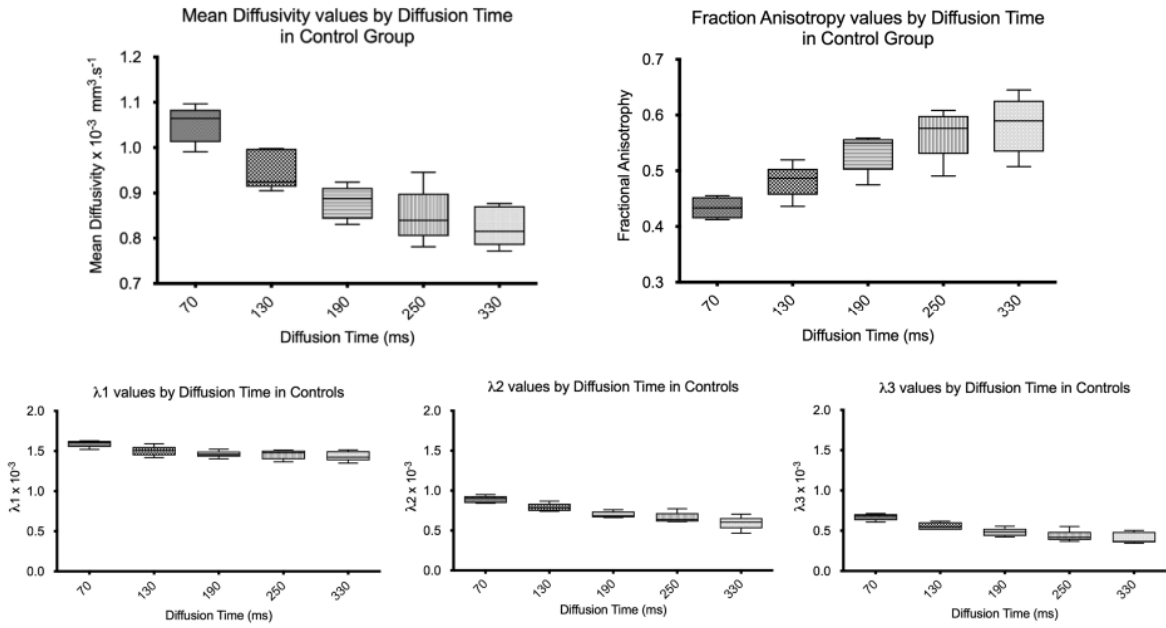
Supporting Information Figure S6: Box-and-whisker plots of the distribution of angular deviation of the principal eigenvector from the spherical mean direction in degrees in healthy volunteers. Whiskers are 5% to 95% percentile.



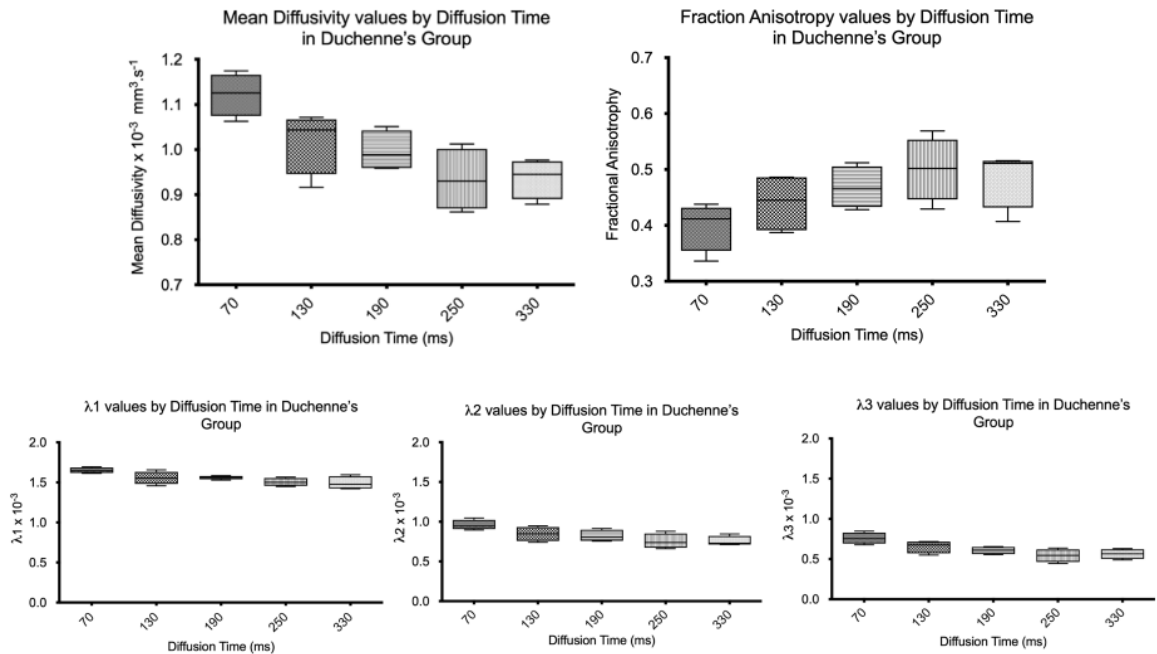
Supporting Information Figure S7: Fat (F), water (W), B0, Mean Diffusivity (MD) and Fractional Anisotropy (FA) images at diffusion time 70ms of all age-matched controls (C) and Boys with Duchenne's (P). Regions of interest are shown on the B0 images.



Supporting Information Figure S8: Example control and patient images for all diffusion times in one control and one boy with DMD (as Figure 3 in main paper). Diffusion times were 70, 130, 190, 250 and 330ms. MD and FA images are scaled identically for all diffusion times (MD $0.0-0.2 \times 10^{-3} \text{ mm}^2 \text{ s}^{-1}$, FA 0.0-0.7)



Supporting Information Figure S9: Box-and-whisker plots of MD, FA and eigenvalues in healthy controls plotted by diffusion time in Tibialis Anterior muscle. Whiskers are 5% to 95% percentile



Supporting Information Figure S10: Box-and-whisker plots of MD, FA and eigenvalues in boys with DMD plotted by diffusion time in Tibialis Anterior muscle. Whiskers are 5% to 95% percentile